JACS
JOURNAL OF THE AMERICAN CHEMICAL SOCIETY

Article

pubs.acs.org/JACS

Mechanistic and Evolutionary Insights from Comparative Enzymology of Phosphomonoesterases and Phosphodiesterases across the Alkaline Phosphatase Superfamily

Fanny Sunden,[†] Ishraq AlSadhan,[†] Artem Y. Lyubimov,[‡] Susanne Ressl,[§] Helen Wiersma-Koch,[†,⊥] Jamar Borland,[†] Clayton L. Brown, Jr.,[†] Tory A. Johnson,[†] Zorawar Singh,[†] and Daniel Herschlag*[,†,∥]

[†]Department of Biochemistry, Beckman Center, Stanford University, Stanford, California 94305, United States

[‡]Departments of Molecular and Cellular Physiology, Neurology and Neurological Science, Structural Biology, and Photon Science, Howard Hughes Medical Institute, Stanford University, Stanford, California 94305, United States

[§]Molecular and Cellular Biochemistry Department, Indiana University, Bloomington, Indiana 47405, United States

[⊥]Department of Biology, Indian River State College, Fort Pierce, Florida 34981, United States

[∥]Departments of Chemical Engineering and Chemistry, and Stanford ChEM-H (Chemistry, Engineering, and Medicine for Human Health), Stanford University, Stanford, California 94305, United States

Supporting Information

ABSTRACT: Naively one might have expected an early division between phosphate monoesterases and diesterases of the alkaline phosphatase (AP) superfamily. On the contrary, prior results and our structural and biochemical analyses of phosphate monoesterase PafA, from *Chryseobacterium meningosepticum*, indicate similarities to a superfamily phosphate diesterase [*Xanthomonas citri* nucleotide pyrophosphatase/phosphodiesterase (NPP)] and distinct differences from the three metal ion AP superfamily monoesterase, from *Escherichia coli* AP (*Ec*AP). We carried out a series of experiments to map out and learn from the differences and similarities between these enzymes. First, we asked why there would be independent instances of monoesterases in the AP superfamily? PafA has a much weaker product inhibition and slightly higher activity relative to *Ec*AP, suggesting that different metabolic evolutionary pressures favored distinct active-site architectures. Next, we addressed the preferential phosphate monoester and diester catalysis of PafA and NPP, respectively. We asked whether the >80% sequence differences throughout these scaffolds provide functional specialization for each enzyme's cognate reaction. In contrast to expectations from this model, PafA and NPP mutants with the common subset of active-site groups embedded in each native scaffold had the same monoesterase:diesterase specificities; thus, the >10^7-fold difference in native specificities appears to arise from distinct interactions at a single phosphoryl substituent. We also uncovered striking mechanistic similarities between the PafA and *Ec*AP monoesterases, including evidence for ground-state destabilization and functional active-site networks that involve different active-site groups but may play analogous catalytic roles. Discovering common network functions may reveal active-site architectural connections that are critical for function, and identifying regions of functional modularity may facilitate the design of new enzymes from existing promiscuous templates. More generally, comparative enzymology and analysis of catalytic promiscuity can provide mechanistic and evolutionary insights.

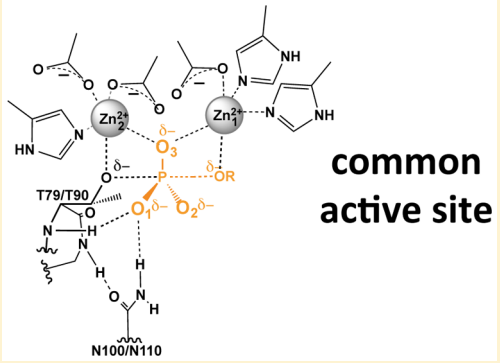

INTRODUCTION

Obtaining a fundamental understanding of how enzymes achieve their enormous rate enhancements and exquisite specificities and elucidating how new enzymes have evolved are central goals of biochemistry. Progress in these areas has biological implications and implications for the ultimate practical goal of effectively and efficiently designing enzymes with new and beneficial activities.

Site-directed mutagenesis, coupled with structural analysis, has been the prevailing approach in enzymology over the past decades. Nevertheless, approaches beyond subtractive site-directed mutagenesis are needed because enzyme energetics are non-additive.[1−16] Our recent quantitative dissection of the functional interplay of five residues in the active site of *Escherichia coli* alkaline phosphatase (*Ec*AP) provided unique mechanistic and evolutionary insights, as well as information that may help guide the design of new enzymes.[17] Nevertheless, enzyme function is also dependent on its overall context, as the enzyme's structure is, of course, needed for catalysis, but it is

Received: June 15, 2016
Published: September 26, 2016

DOI: 10.1021/jacs.6b06186
J. Am. Chem. Soc. 2016, 138, 14273−14287

Chart 1. Substrates Used in This Study

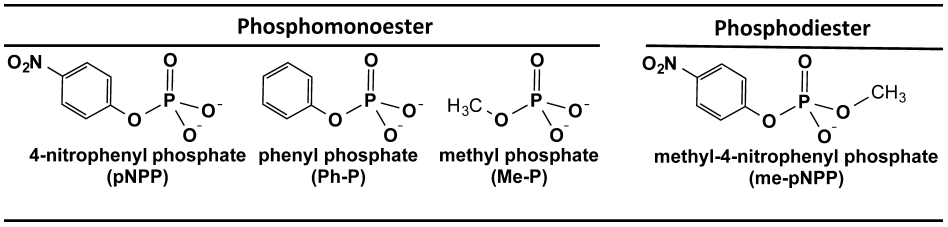

not yet practical to comprehensively dissect the interconnections between active-site residues and the sea of surrounding residues and structural elements.

Given the natural complexities of enzymes and these practical limitations, the study of enzyme superfamilies has been enormously valuable. These studies have identified common and potentially critical structural and catalytic elements and, conversely, suggested residues and structural features that may allow individual enzymes to specialize in different reactions (e.g., refs 18−20). Of particular utility is the observation that enzymes across a superfamily often exhibit low but substantial activity for reactions of other superfamily members, a property referred to as 'catalytic promiscuity.[21,22] Catalytic promiscuity can be used as a comparative tool in elucidating mechanism and as a probe of factors that may have influenced enzyme evolution (see refs 23 and 24).

The alkaline phosphatase (AP) superfamily has been particularly amenable to comparative studies, as members exhibit promiscuity for multiple reactions catalyzed by other superfamily members.[24−35] We compare PafA, a phosphate monoesterase from *Chryseobacterium meningosepticum*, with two other enzymes within the AP superfamily that share its Zn^{2+} bimetallo core, one catalyzing the same reaction and the other catalyzing phosphate diester hydrolysis. Intriguingly, the PafA monoesterase has similarities to superfamily phosphate diesterases and differences from the three metal ion AP superfamily monoesterases such as *Ec*AP. These observations raise intriguing evolutionary questions and provide compelling opportunities to obtain mechanistic insights via comparative enzymology and analysis of catalytic promiscuity.[32]

EXPERIMENTAL SECTION

Plasmid Design. *C. meningosepticum* expresses the alkaline phosphatase gene *pafA*. This gene has been modified with a sequence expressing a C-terminal strepII tag with a Factor Xa cleavage site between the tag and the natural C-terminal end. The gene was cloned into a pET22b vector (Supporting Information S1). Control experiments with and without the strepII-tag removed from expressed wild-type (WT) PafA suggest that the tag has no effect on catalysis; the tag was therefore retained in the kinetic experiments but cleaved for crystallization.

Expression and Purification of PafA and NPP. PafA was expressed from *E. coli* SM547(DE3) cells containing the PafAstrepII construct. The cells were grown to an optical density of 0.6−0.8 OD_{600} in rich medium and glucose (10 g of tryptone, 5 g of yeast extract, 5 g of NaCl, and 2 g of glucose per liter) with 50 mg/L carbenicillin at 37 °C. To induce protein expression, Isopropyl thiogalactopyranoside (IPTG) was added to a final concentration of 0.3 mM. The cultures were further grown at 30 °C for 16−20 h and were harvested by centrifugation. The pellets were resuspended in column buffer (100 mM Tris-HCl, pH 8.0, 150 mM NaCl, and 10 μM $ZnCl_2$) and either frozen for later purification or lysed by passing the suspension through an EmulsiFlex-C5 apparatus (Avestin, Ottawa, ON) three times. The lysate was cleared from cell debris by centrifugation (20000*g*, 20 min), and the supernatant was filtered through a 0.45 μm filter. The filtrate was loaded over a 1 mL gravity column containing *Strep*-Tactin Superflow resin (IBA Life Sciences, Göttingen, Germany). The resin was washed with 6 column volumes of column buffer, and the protein was eluted with 2.5 mM desthiobiotin in column buffer. The purity of the PafA-containing fractions were assessed with sodium dodecyl sulfate−polyacrylamide gel electrophoresis (SDS-PAGE) and was >95% pure as estimated by staining with Coomassie Blue. Fractions containing purified PafA were pooled and buffer exchanged into storage buffer (10 mM sodium MOPS, pH 8.0, 50 mM NaCl, and 100 μM $ZnCl_2$).

Mutant F91A/L123A/Y205A of NPP, from *Xanthomonas axonopodis* pv *citri*, was expressed and purified from a construct containing an N-terminal maltose binding protein (MBP) fusion and C-terminal strepII tags with a Factor Xa cleavage site between it and the natural C-terminal end of NPP, as previously described.[36] The NPP mutant was expressed and purified over a *Strep*-Tactin Superflow column as described above for PafA. Fractions containing purified NPP were pooled and buffer exchanged into storage buffer (100 mM sodium MOPS, pH 8.0, 150 mM NaCl, and 100 μM $ZnCl_2$).

Kinetic Assays of PafA Variants. Activity measurements for all enzymes were performed at 25 °C in a Perkin-Elmer UV/vis Lambda 25 spectrophotometer (Perkin Elmer, Waltham, MA) in 0.1 M sodium MOPS (or/and Tris-HCl), pH 8.0, 0.5 M NaCl, 100 μM $ZnCl_2$, unless otherwise noted. Hydrolysis of the substrates containing a *p*-nitrophenolate leaving group (pNPP and me-pNPP, Chart 1) were followed by assaying the formation of free *p*-nitrophenolate continuously at 400 nm (Scheme 1). Rate constants were determined

Scheme 1. Reaction Scheme for Phosphate Ester Hydrolysis

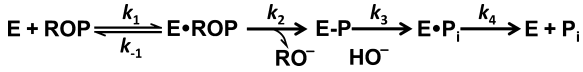

from initial rates, and the activity of the free enzyme, k_{cat}/K_M, was determined. The kinetic parameters were shown to be first-order in both enzyme and substrate concentration, with concentrations varied over at least a 5-fold range. For pNPP, substrate concentrations high enough to obtain K_M and k_{cat} values were achievable, and these values are also reported; the concentration of pNPP was varied at least 5-fold below and above the measured K_M in all cases. The following pNPP concentrations were used: WT, 2.0×10^{-2}−2.5 mM; T79S, 0.55−110 μM; K162A, 1.1×10^{-3}−2.5 mM; R164A, 1.1×10^{-3}−4.5 mM. Fits had R^2 values of >0.98 in all cases. Reported errors were estimated from at least two independent kinetic measurements. Comparisons with independent enzyme preparations for each of the PafA mutants gave values within the reported error.

The K_M value for pNPP of the N100A mutant was too low to measure directly at pH 8.0. We therefore used an indirect method described previously.[24] Briefly, we used an inhibitor (tungstate), whose inhibition constant was determined using a substrate with a much higher K_M (me-pNPP), to raise the observed K_M value in these pNPP reactions. Apparent values for k_{cat} and K_M were obtained at 2.1, 6.3, and 12.5 mM tungstate. As expected for competitive inhibition, the k_{cat} values were constant (and the same as obtained in the absence of tungstate), and the observed K_M values increased with increasing tungstate concentration. From these observed values, K_M for the pNPP reaction was calculated using eq 1, the measured $K_{M,apparent}$, and the independently determined K_i.

DOI: 10.1021/jacs.6b06186
J. Am. Chem. Soc. 2016, 138, 14273−14287

$$K_{M,apparent} = \frac{K_M}{1 + [I]/K_i} \quad (1)$$

Values of k_{cat}/K_M for Me-P (Chart 1) were obtained using a discontinuous kinetic assay, following the formation of free phosphate by a Malachite green assay (as described in ref 37). For the N100A and T79S mutants, the K_M was too low, given the sensitivity of this assay to obtain reliable k_{cat}/K_M values. Tungstate could not be used as above to raise the K_M and allow determination of k_{cat}/K_M because the Malachite Green assay is not compatible with tungstate. We therefore measured the activity of these mutants at pH 9.0, where the K_M is higher, and extrapolated to pH 8.0 using the ratio of pNPP k_{cat}/K_M values at pH 8.0 and pH 9.0 (eq 2; Supporting Information S2). As a control, the same measurements were carried out for WT PafA, and the measured and calculated values agreed within 2-fold.

$$\left(\frac{k_{cat}}{K_M}\right)_{Me\text{-}P,pH\,8} = \frac{(k_{cat}/K_M)_{pNPP,pH\,8}}{(k_{cat}/K_M)_{pNPP,pH\,9}}\left(\frac{k_{cat}}{K_M}\right)_{Me\text{-}P,pH\,9} \quad (2)$$

Hydrolysis rates for phenyl phosphate (Ph-P) were measured by following production of free phenol. Production of free phenol was assayed as phenolate by taking aliquots of the reaction at specified time points and quenching in equal volume of 0.1 M sodium hydroxide. Absorbance was measured at 278 nm with 500 nm as a reference wavelength on a Tecan Infinite 200 PRO Microplate Reader (Tecan, Männedorf, Switzerland), against a standard curve of phenol (Sigma-Aldrich, St. Louis, MO).

The following buffers were used for pH dependences: MES (pH 6.0), MOPS (pH 7.0), CHES (pH 9.0), CAPS (pH 10.0) at 100 mM, each as a sodium salt in the presence of 500 mM NaCl and 100 μM $ZnCl_2$, to ensure that there were no changes in pH-dependences or protonation states introduced by the mutations (Supporting Information S2).

Inhibition constants were determined for tungstate, vanadate, and inorganic phosphate (P_i) in 0.1 M sodium MOPS, pH 8.0, 0.5 M NaCl, 100 μM $ZnCl_2$, using subsaturating concentrations of me-pNPP (Chart 1). The following inhibitor concentrations were used: WT, 0.16−28 μM vanadate, 1.6×10^{-4}−13 mM tungstate, 0.13−5.0 mM P_i; T79S, 16−450 μM vanadate, 6.3×10^{-2}−13 mM tungstate, 6.3×10^{-3}−1.2 mM P_i; N100A, 6.3×10^{-2}−13 mM vanadate, 6.3×10^{-2}−13 mM tungstate, 0.2−13 mM P_i; K162A, 16−450 μM vanadate, 6.3×10^{-2}−13 mM tungstate, 0.38−13 mM P_i; R164A, 1.6×10^{-2}−13 mM vanadate, 6.3×10^{-2}−13 mM tungstate, 0.38−13 mM P_i.

Inhibition constants for vanadate were also measured with pNPP for WT PafA and the T79S, K162A, and R164A mutants to test if the observed activity arose from the same active site (Supporting Information S3). As the K_M for pNPP hydrolysis by N100A PafA at pH 8.0 is very small, the K_i for tungstate was measured at pH 9.0 (0.1 M sodium CHES, 0.5 M NaCl, 100 μM $ZnCl_2$) for me-pNPP and pNPP. The inhibition constant was calculated with a non-linear least-squares fit to the data using eq 3 for competitive inhibition.

$$\left(\frac{k_{cat}}{K_M}\right)_{apparent} = \frac{(k_{cat}/K_M)}{1 + [I]/K_i} \quad (3)$$

Accounting for Non-chemical Rate-Limiting Steps and Limits in k_{cat}/K_M Measurements. As previously observed for WT *Ec*AP,[38] the k_{cat}/K_M values for pNPP by WT PafA and a subset of its mutants are within the range observed when substrate binding, rather than a chemical step, is rate limiting. To allow comparisons of catalysis by PafA and its mutants that assess the ability of these enzymes to carry out the chemical step, we used information from intrinsically less reactive substrates so that comparisons reflect effects on substrate binding and the subsequent chemical step and not simply association kinetics. We followed the approach previously taken by O'Brien et al. for *Ec*AP.[34,38]

In principle we could obtain and compare k_{cat}/K_M values for all PafA variants with a poorly reactive substrate, and thereby avoid any need to correct values for pNPP or other more activated substrates. However, reactivity of the least reactive PafA mutant, K162A, was too low to measure with Me-P. Nevertheless, we were able to obtain an upper limit for this mutant with Me-P and k_{cat}/K_M values for all of the other PafA variants, and all of the conclusions herein could be made by these comparisons alone. Further, we used comparisons between substrates of differing intrinsic reactivity to obtain a $(k_{cat}/K_M)_{Me\text{-}P}$ estimate for K162A PafA relative to the other variants. The only underlying assumption is that each variant has the same ratio of chemical catalysis for the substrates, and this assumption is supported by comparisons of several variants and substrates (Supporting Information S4).

Occupancy of Metals and Phosphate in the PafA Active Site and Structure. To test for possible metal ion concentration dependent activation, such as observed for *Ec*AP mutant E322Y,[24] WT PafA was incubated with the following metal concentrations: 10 μM $ZnCl_2$, 100 μM $ZnCl_2$, 500 μM $ZnCl_2$, 1.0 mM $MgCl_2$ and 100 μM $ZnCl_2$ in 10 mM sodium MOPS, pH 8.0, and 50 mM NaCl at 25 °C. No activation was observed after a week of incubation. The occupancy of metals and phosphorus in the WT PafA active site was determined with atomic emission spectroscopy as described previously.[24] The following ratios were obtained: Zn^{2+}:protein = 3.1; Mg^{2+}:protein = 0.012; Ca^{2+}:protein = 0.53; P_i:protein = 2.9. The metal ion occupancies suggested that Mg^{2+} does not bind to the PafA active site, consistent with the lack of activation by 1 mM $MgCl_2$. The Zn^{2+} value is consistent with occupancy of the Zn^{2+}-bimetallo site and partial occupancy of one or both of the remote Zn^{2+} sites observed in the crystal structure (see below). Although the results suggest half occupancy of a Ca^{2+} ion, addition of Ca^{2+} (1 mM) did not increase activity.

Crystallization and Crystallographic Data Collection for WT PafA. The affinity tag was cleaved from PafA by incubating WT PafA with factor Xa (New England BioLabs, Ipswich, MA) for 4 days in 50 mM Tris-HCl, pH 8.0, 200 mM NaCl, 10 mM maltose, 5 mM $CaCl_2$. PafA was buffer exchanged into 10 mM Tris-HCl, pH 8.0, 50 mM NaCl, 100 μM $ZnCl_2$ and concentrated to 2.5 mg/mL. Crystal growth was achieved via the hanging drop method using vapor diffusion where equal volumes of PafA and precipitant solution (22% polyethylene glycol (PEG) MW 3350, 0.1 M sodium acetate, pH 4.4, 0.2 mM ammonium sulfate) were mixed on a cover slide and placed over a reservoir of 1 mL of precipitant solution at room temperature. Crystals were harvested using nylon loops (Hampton Research, Aliso Viejo, CA) or LithoLoops (Molecular Dimensions Inc., Altamonte Springs, FL) and immediately flash frozen into liquid nitrogen; the high concentration of PEG MW 3350 in the precipitation solution was determined to be sufficient for cryopreservation. Crystallographic data were collected at the Stanford Synchrotron Radiation Laboratory (SSRL) Beamline 11-1. Radiation sensitivity of the crystals was immediately apparent during data collection, as the overall intensity of recorded reflections decreased with concurrent rapid increase of mosaicity after ~20−40 5-second exposures. To alleviate this problem, we collected data sets from seven PafA crystals and merged high-quality frames into a single data set.

Processing of Diffraction Data and Structure Determination. Raw diffraction images were indexed and integrated using iMosflm,[39,40] followed by a merging and scaling step using *Pointless* and *Aimless*.[41] The final merged data set included ~20−40 initial frames from each of the seven separate crystals and extended to 1.7 Å. The L-test[42] detected significant twinning, with the twin fraction of 0.242; as a result, the merging R-values appear somewhat inflated. The final merging statistics are provided in Table 1. The structure was solved by molecular replacement (MR) using Phaser,[43,44] with the modified structure of SPAP (PDB ID: 3Q3Q) used as a search model. MR was successful only when most of the divergent regions were omitted, with essentially the conserved alpha-beta core retained in the search model. The maps were steadily improved with multiple rounds of incremental manual modeling of the best-resolved portions in Coot[45] alternating with automated refinement in *phenix.refine*.[46] A set of twin operators $(-h, -k, -l)$ was utilized throughout the refinement. The final model included nearly the entire expressed PafA monomer, with the exception of 12 residues of the N-terminus and 1 residue of the C-terminus. At this stage, clear electron density could be seen for the two active-site Zn^{2+} ions as well as two additional Zn^{2+} sites at the

DOI: 10.1021/jacs.6b06186
J. Am. Chem. Soc. 2016, 138, 14273−14287

Table 1. X-ray Crystallographic Data Collection and Refinement Statistics

Data Collection	
space group	*I*4
unit cell axes	
a, *b*, *c* (Å)	113.8, 113.8, 71.4
α, *β*, *γ* (deg)	90, 90, 90
resolution range (Å)	36.0−1.7
R_{merge} (%)	28.7 (50.0)
R_{pim} (%)	13.1 (52.0)
$\langle I\rangle/\langle\sigma I\rangle$	8.4 (3.2)
completeness (%)	96.6 (85.3)
multiplicity	5.4 (1.9)
$CC_{1/2}$	95.8% (41.6%)

Refinement	
resolution range (Å)	36.0−1.7
no. unique reflections	48541 (4475)
R_{work}/R_{free} (%)	15.9/17.7
no. atoms	4771
average *B*-factors (Å^2)	
protein	13.1
water	29.4
ligands	40.9
rms deviation from ideality	
bond length (Å)	0.003
bond angles (deg)	0.62
Ramachandran statistics	
favored regions (%)	97.2
allowed regions (%)	2.4
outliers (%)	0.4
PDB code	5TJ3

PafA exterior. Once these were modeled, a strong residual electron density feature in the active site could be identified as a phosphate moiety covalently attached to Thr79. The final model converged with R_{work}/R_{free} of 15.9%/17.7%, are lower than typical for structures at this resolution (as reported by the Phenix statistical tool[47]), as a result of twinning.[48] The model exhibited good stereochemistry and reasonable refinement statistics as per Molprobity[49] as well as the Polygon tool[47] in the Phenix suite of software.[46] Refinement statistics are summarized in Table 1.

PafA, EcAP, and NPP Sequence Comparisons. EMBOSS Stretcher was used to align the amino acid sequence translated from the genes for PafA (UniProtKB/Swiss-Prot: AF157621.2) with SPAP (UniProtKB/Swiss-Prot: A1YYW7.1), NPP (UniProtKB/Swiss-Prot: AAM37669.1), and *Ec*AP, (UniProtKB/Swiss-Prot: AAG54729.1) using BLOSUM 62 (see Supporting Information S5). Structures were overlaid using the Chimera[50] alignment tool Matchmaker. The following PDB codes were used: SPAP, 3Q3Q; *Ec*AP, 1ALK; and NPP, 2RH6, using the Smith−Waterman algorithm (local), BLOSUM-50, and a secondary structure score of 80%. The structural alignment was used to make a multiple sequence alignment (Supporting Information S5).

RESULTS

The PafA Structure. Crystals of PafA were obtained, and its structure was determined to 1.7 Å resolution (Table 1). As expected based on sequence similarities, its core architecture matches that of *Ec*AP, NPP, and other members of the AP superfamily (Figure 1A,B, gray and white), and its Zn^{2+} bimetallo center is highly homologous to those of NPP and *Ec*AP (Figure 2; see Supporting Information S5 for a structure-based sequence alignment).

The overall structure and active-site configuration of PafA closely match those of *Sphingomonas* sp. BSAR-1 (SPAP), an AP superfamily member closely related to PafA (Supporting Information S6). As noted by Bihani et al., SPAP shares specific active-site features with the AP superfamily phosphodiesterases such as NPP.[51] These similarities are also seen with PafA (Figure 2). PafA, SPAP, and NPP share a nucleophilic threonine, while *Ec*AP has a serine, and PafA, SPAP, and NPP contain a homologous active-site asparagine that appears to make identical interactions with oxygen atom (O_1) of the transferred phosphoryl group (Figure 2, Scheme 2, Supporting Information S5). *Ec*AP lacks this asparagine residue, and, although the PafA, SPAP, and *Ec*AP active sites all have arginine and lysine residues, the arginine and lysine residues in the *Ec*AP active site originate from distinct helices and loops and make distinct interactions (Figures 1B and 2, Supporting Information S5 and S6, ref 51).

PafA was previously isolated and expressed by Berlutti et al.,[52] and initial structure−function studies were carried out by Bihani et al. with SPAP.[51,53] Our studies build upon this prior research and are consistent with their results.

PafA's Reaction Specificity for Phosphate Monoester versus Diester Hydrolysis. Based on structural inspection, SPAP and PafA are expected to be phosphate monoesterases, as they lack a binding pocket for the second diester substituent and have positively charged residues situated to interact with both non-bridging oxygen atoms of phosphomonoester substrates (Figure 2, Supporting Information S6, ref 51). To formally test this expectation, we followed the PafA hydrolysis of phosphate monoester and diester substrates, pNPP and me-pNPP, respectively (Chart 1). We observed a preference of ~10^5-fold for catalysis of the monoester reaction (Table 2, WT). This value represents a lower limit for the preferential chemical catalysis, as binding rather than the chemical step appears to be rate limiting for the pNPP reaction (see Experimental Section, Accounting for Non-chemical Rate-Limiting Steps and Limits in k_{cat}/K_M Measurements, and Supporting Information S4), and as the methyl substituent of the diester substrate does not make binding interactions made with substituents of physiological diesterase substrates.[24,32,54]

Effect of Active-Site Mutations on PafA Catalysis. We next assessed the effect of PafA active-site mutations on the phosphate monoesterase and diesterase activities. Each PafA active-site residue that appears to contact the phosphoryl group, N100, K162, and R164, was mutated to alanine, and the nucleophilic threonine residue, T79, was mutated to serine. Values of k_{cat}/K_M were first determined with a *p*-nitrophenoxide leaving group (Table 2; pNPP and me-pNPP, Chart 1). Whereas the diester reactions were uniformly slow, and thus very likely limited by the chemical step, the high k_{cat}/K_M values of ~10^6 M^{-1} s^{-1} for pNPP, the monoester substrate, were within the range seen for rate constants for substrate binding to enzymes.[55] Furthermore, mutations that gave 20−200-fold effects on the non-cognate diesterase reaction had essentially no effect on the cognate monoesterase reaction for a subset of the mutations (Table 2, i.e., T79S and N100A). This result is most simply accounted for by a non-chemical rate-limiting step that masks effects on the chemical step for the pNPP monoester reaction for WT PafA (Supporting Information S4).

To further investigate the effects of the mutations on phosphomonoester hydrolysis we therefore carried out reactions for each PafA variant with less reactive phosphate monoester substrates, phenyl phosphate (Ph-P) and methyl

DOI: 10.1021/jacs.6b06186
J. Am. Chem. Soc. 2016, 138, 14273−14287

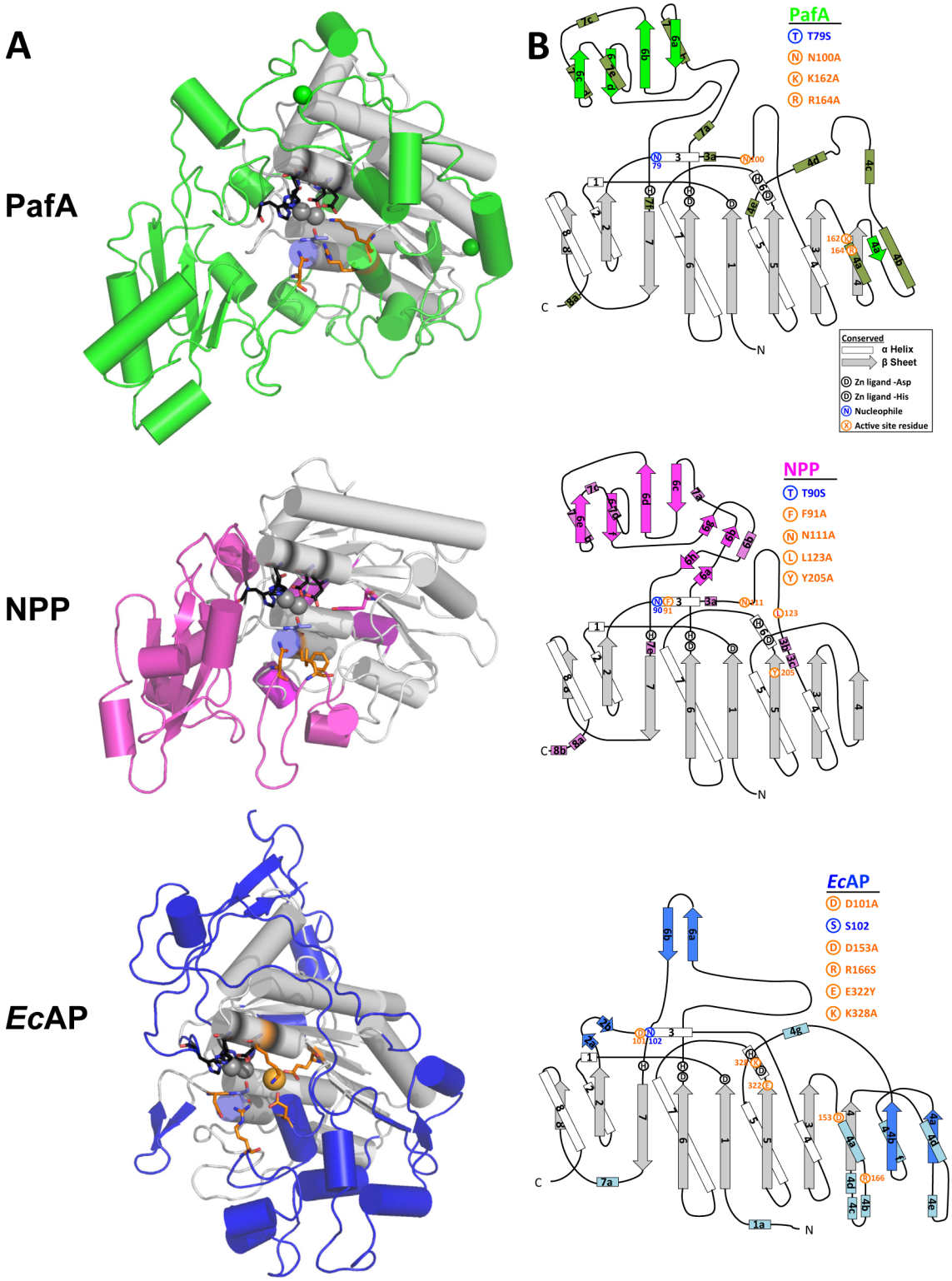

Figure 1. Global structure and active site of PafA, NPP, and *Ec*AP. (A) Comparison of the global structure of PafA, NPP, and *Ec*AP. The structurally conserved core and bimetallo Zn^{2+} (spheres) are shown in gray, conserved zinc ligands are shown in black, and auxiliary domains that are not conserved between all three enzymes are shown in color; PafA in green, NPP in magenta, and *Ec*AP in blue. The active-site nucleophile (threonine or serine) is shown in blue, and other active-site residues and *Ec*AP Mg^{2+} (sphere) are shown in orange. (B) Topographic diagrams for PafA, NPP, and *Ec*AP, with arrows representing β-sheets and rods representing α-helices. Gray represents conserved sheets and white conserved helices, and the auxiliary regions that are not conserved between all three enzymes are colored: PafA, helices in olive, sheets in green; NPP, helices in purple, sheets in magenta; and *Ec*AP, helices in light blue, sheets in blue. Structures are from 3tg0 (*Ec*AP,[96]) and 2gso (NPP,[32]) with ligands removed for clarity.

phosphate (Me-P; Chart 1, Table 3). The larger mutational effects observed with the less reactive substrates supported the model of rate limiting binding for reaction of pNPP with the faster mutants. Hence, we used Me-P to compare the PafA

DOI: 10.1021/jacs.6b06186
J. Am. Chem. Soc. 2016, 138, 14273−14287

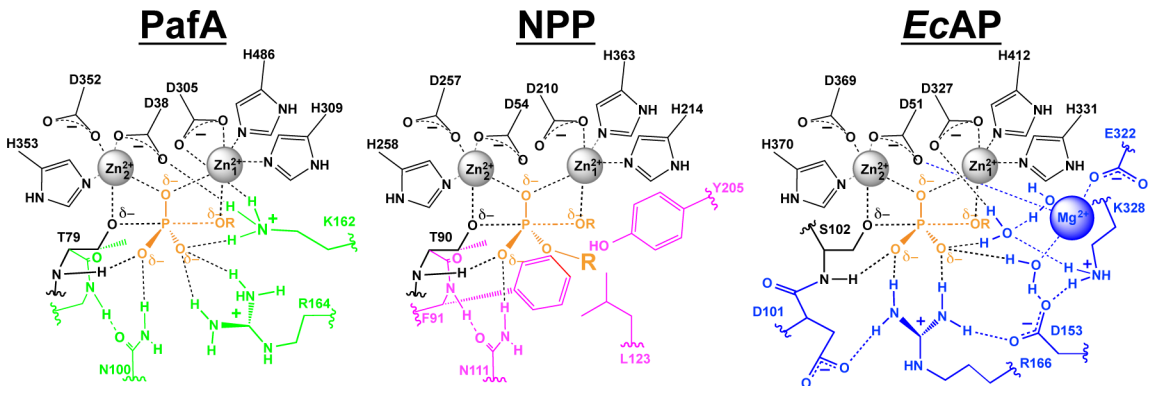

Figure 2. Active-site schematics for PafA, NPP, and *Ec*AP. The enzymes have a conserved bimetallo core (black, including the threonine or serine nucleophile), conserved zinc ligands (gray), and additional non-universally conserved active-site residues, which are colored for each enzyme. The phosphoryl group, in orange, is shown with partial bonding to the nucleophile and its leaving group (OR), corresponding to the reaction's presumed transition state.

Scheme 2. Transition-State Model for Alkaline Phosphatase Superfamily Reactions

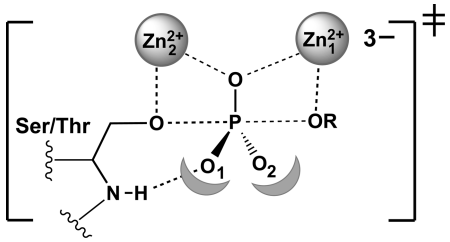

mutants. As only an upper limit could be obtained for the Me-P reactivity of the most affected mutant (K162A), we used the observed constant ratio of reactivity of the different substrates to estimate this k_{cat}/K_M value (see Experimental Section and Supporting Information S4); use of this value rather than the limit does not affect the conclusions drawn herein.

Given the uniformly low k_{cat}/K_M values with the phosphate diester substrate, additional precautions and controls are required to ensure that a contaminant that is physically undetectable, but highly proficient at the alternative reaction, does not account for the observed promiscuous activity. We therefore determined inhibition constants for the phosphate monoester and diester reactions (Supporting Information S3). For each PafA variant, the same inhibition constant was observed for the phosphate mono- and diester reactions, suggesting that catalysis of both reactions arises from the same active site. Also, different inhibition constants were observed for different mutants, providing further support for the conclusion that the promiscuous diesterase activities arose from PafA and its variants (Table 4).

Effect of Active Site Mutations on Binding of Ground- and Transition-State Analogues. For WT PafA and each of the active-site mutants, we determined the inhibition constants for P_i and for two potential transition-state analogues, vanadate and tungstate (Table 4). The T79S mutation, which decreases catalysis (Table 2) and, correspondingly, decreases binding of both transition-state analogues, lead to an *increase* in P_i affinity (Table 4, decreased K_i). The paradoxical stronger binding accompanied by weaker catalysis is accounted for by an electrostatic destabilization model, akin to that observed for *Ec*AP,[56,57] as described in the Discussion. There is also a remarkable congruence of the mutational effects on activity and binding of these ligands to PafA and *Ec*AP, despite the lack of conservation between the mutated residues, as also described in the Discussion.

Comparative Enzymology of PafA versus NPP. As noted by Bihani et al. for SPAP, and emphasized above for PafA, these phosphate monoesterases share significant homology with AP superfamily diesterases such as NPP, despite their specialization to catalyze a different reaction (Figures 1 and 2, Table 2). Accordingly, we created mutant versions of PafA and NPP that remove the active-site residues that are distinct between these enzymes and retain the common Zn^{2+} bimetallo center, threonine nucleophile, and active-site asparagine, and then we compared their activities (Figure 3A). For diesterase activity, we used me-pNPP, as its methyl substituent minimizes interactions between the substituent of the transferred phosphoryl group and the diesterase (NPP) binding site for this substituent.[32,36] Whereas wild-type PafA and NPP show large preferences for monoester and diester substrates, respectively (Figure 3B,C), the mutants of each show no significant preference (≤3-fold) between these reactions and

Table 2. PafA Phosphomonoesterase and Diesterase Reaction Kinetics[a]

	pNPP				me-pNPP[c]		$(k_{cat}/K_M)_{pNPP}$
enzyme	k_{cat}/K_M (M^{-1} s^{-1})	k_{rel}[b]	K_M (M)	k_{cat} (s^{-1})	me-pNPP (M^{-1} s^{-1})	k_{rel}[b]	$(k_{cat}/K_M)_{Me\text{-}pNPP}$
WT	$1.6(0.4) \times 10^6$	(1)	$1.9(0.4) \times 10^{-4}$	3.0×10^2	$1.7(0.5) \times 10^1$	(1)	9.4×10^4
T79S	$6.3(1.5) \times 10^5$	2.5	$2.9(0.3) \times 10^{-6}$	1.8	$6.6(2.2) \times 10^{-1}$	26	9.5×10^6
N100A	$7.6(2.0) \times 10^5$	2.1	$5.1(1.3) \times 10^{-7}$	3.9×10^{-1}	$1.1(0.4) \times 10^{-1}$	1.5×10^2	6.9×10^6
K162A	$1.3(0.1) \times 10^2$	1.2×10^4	$2.3(0.8) \times 10^{-4}$	3.0×10^{-2}	$1.3(0.1) \times 10^1$	1.3	1.0×10^1
R164A	$1.3(0.4) \times 10^5$	1.2×10^1	$5.1(1.5) \times 10^{-5}$	6.6	$1.4(0.1) \times 10^1$	1.2	9.3×10^3

[a]Assay conditions: 100 mM sodium MOPS, pH 8.0, 500 mM NaCl, 100 μM $ZnCl_2$. [b]k_{rel} values are k_{cat}/K_M for WT divided by k_{cat}/K_M for each mutant. By definition the value for WT PafA is one. [c]$(K_M)_{Me\text{-}pNPP} \gg 1.0$ mM for WT and all mutants.

DOI: 10.1021/jacs.6b06186
J. Am. Chem. Soc. 2016, 138, 14273−14287

Table 3. k_{cat}/K_M Values for Phosphomonoester Hydrolysis by WT and Mutant PafA Enzymes[a]

enzyme	pNPP[a] (M^{-1} s^{-1})	k_{rel}[b]	Ph-P[a] (M^{-1} s^{-1})	k_{rel}[b]	Me-P[a] (M^{-1} s^{-1})	k_{rel}[b]
WT	$1.6(0.4) \times 10^6$	(1)	$8.3(1.2) \times 10^5$	(1)	$8.5(0.6) \times 10^4$	(1)
T79S	$6.3(1.5) \times 10^5$	2.5	1.4×10^5[b]	5.9	3.8×10^3[b]	22
N100A	$7.6(2.0) \times 10^5$	2.1	1.5×10^5[b]	5.5	2.2×10^2[b]	3.9×10^2
K162A	$1.3(0.1) \times 10^2$	1.2×10^4	8.2(0.1)	1.0×10^5	1.8×10^{-2}[c]	4.7×10^6
R164A	$1.3(0.4) \times 10^5$	1.2×10^1	$1.0(0.3) \times 10^4$	8.3×10^1	$4.2(0.3) \times 10^1$	2.0×10^3

[a]Assay conditions: 100 mM sodium MOPS, pH 8.0, 500 mM NaCl, 100 μM $ZnCl_2$, unless annotated (pH 9.0) for which 100 mM sodium CHES, pH 9.0, 500 mM NaCl, 100 μM $ZnCl_2$ was used. [b]k_{cat}/K_M was measured at pH 9.0 rather than pH 8.0 for these substrates and mutants, as the low K_M values at pH 8.0 prevented measurement of accurate k_{cat}/K_M values. The k_{cat}/K_M at pH 8.0 were estimated using the ratio of k_{cat}/K_M for pNPP at pH 8.0 and pH 9.0, as described in the Experimental Section (see Kinetic Assays of PafA Variants). The pH 9.0 rate constants are given in Supporting Information Table S4. [c]Estimated assuming constant ratios of reactivity ratios for the substrates as described in the Experimental Section (see Accounting for Non-chemical Rate-Limiting Steps and Limits in k_{cat}/K_M Measurements). The measured limit is $\leq 2.0 \times 10^{-1}$ M^{-1} s^{-1}.

Table 4. Inhibition of WT and Mutant PafA by Ground- and Transition-State Analogues[a]

	P_i		tungstate		vanadate	
enzyme	K_i (mM)	K_{rel}	K_i (mM)	K_{rel}	K_i (mM)	K_{rel}
WT	$8.3(1.0) \times 10^{-1}$	(1)	$3.9(0.1) \times 10^{-3}$	(1)	$6.7(0.4) \times 10^{-4}$	(1)
T79S	$9.6(0.4) \times 10^{-3}$	1.2×10^{-2}	$2.8(0.8) \times 10^{-1}$	7.2×10^1	$9.0(0.2) \times 10^{-2}$	1.3×10^2
N100A	1.3(0.2)	1.6	$5.7(2.3) \times 10^{-1}$	1.5×10^2	$1.9(0.1) \times 10^{-1}$	2.8×10^2
K162A	4.7(1.2)	5.7	>13	$>3.3 \times 10^3$	$7.9(2.6) \times 10^{-2}$	1.2×10^2
R164A	>13	>16	1.3(0.4)	3.3×10^2	$3.0(0.7) \times 10^{-1}$	4.5×10^2

[a]Conditions: 100 mM sodium MOPS, pH 8.0, 500 mM NaCl, 100 μM $ZnCl_2$. Obtained as described in Experimental Section.

also exhibit extensive catalysis of $\sim 10^{12}$-fold for both reactions (Table 5).

DISCUSSION

Enzymes of the AP superfamily catalyze a range of reactions, with its bimetallo branch containing phosphate monoesterases and diesterases, along with phosphomutases and phosphonoacetate hydrolases.[24−27,32,33,58,59] Naively, one might expect an early division between phosphate monoesterase and diesterase superfamily members, such that there would be similarities between all monoesterases and persistent distinctions between these enzymes and the diesterases. However, PafA and SPAP are phosphate monoesterases with similarities to superfamily phosphate diesterases and differences from the three metal ion AP superfamily monoesterases such as *E. coli* AP (*Ec*AP) (Figures 1 and 2; Supporting Information S6; ref 51, comment 60). These observations raised intriguing evolutionary questions and provided us with compelling opportunities to obtain mechanistic insights via comparative enzymology and analysis of catalytic promiscuity.[32]

Evolution of Phosphate Monoesterases with Distinct Functional Properties. Why are there AP superfamily phosphate monoesterases with distinct active-site architectures, and why would one more resemble the AP superfamily phosphate diesterases? *Ec*AP comes from a gut bacteria (*E. coli*), whereas PafA is derived from a bacterium found in soil and salt and fresh water (*C. meningosepticum*).[52,61] Further, phosphate is often a scarce resource for growth, and there is complex regulation of P_i uptake and storage and roles of phosphate in stress and pathogenesis.[62,63] The different catalytic constants we observe for PafA and *Ec*AP are consistent with different metabolic evolutionary pressures, arising from different lifestyles that favored distinct active-site architectures.

*Ec*AP exhibits very strong product inhibition by P_i, with a K_i in the low micromolar and more than 3 orders of magnitude stronger than that for PafA (Figure 4A). The strong binding could be functional—for example, limiting enzyme turnover until P_i that has been produced can be cleared from the periplasm and utilized. Alternatively, the strong product inhibition may be a necessary trade-off to achieve the ~4-fold higher k_{cat}/K_M for *Ec*AP relative to PafA (Figure 4B).[64]

While it is always possible that the functional differences between *Ec*AP and PafA arose from trapping of a suboptimal evolutionary solution as a local maximum on the enzyme's fitness landscape for one of enzymes, there is also an intriguing possibility that *E. coli* and a subset of other bacteria utilize strong product inhibition for phosphate homeostasis and signaling in ways that remain to be elucidated. Our results open new biological questions that would be indiscernible without quantitative comparative enzymology.

Modular Active-Site Architecture Facilitates Transitions between AP Superfamily Phosphate Monoesterases and Diesterases. Within the *Ec*AP active site, R166 interacts with both of the phosphoryl oxygen atoms that face away from the Zn^{2+} bimetallo site (Figure 2). Consistent with this structural picture, mutation of R166 is deleterious for both phosphate monoesterase and diesterase reactions but is more deleterious for monoesterase reactions.[24] Thus, if R166 of *Ec*AP were mutated to allow the introduction of residues that interact with a diester R′ substituent, interactions with the other, non-esterified oxygen atom would be compromised, and the promiscuous diester reaction would be adversely affected. Based on these observations, the *Ec*AP active-site architecture would be expected to impede evolutionary transitions between mono- and diesterases, and these observations may account for the absence of diesterase superfamily members that are highly related to *Ec*AP. For analogous reasons, *Ec*AP might be a suboptimal starting point for engineering a new phosphodiesterase.

In contrast, residues within PafA's active site interact with *either* of the two phosphoryl oxygen atoms facing away from the Zn^{2+} bimetallo center (O_1 and O_2 in Scheme 2). Oxygen atom O_1 accepts hydrogen bonds from the side chain of N100 and the backbone amide of T79 (the active-site nucleophile), and

DOI: 10.1021/jacs.6b06186
J. Am. Chem. Soc. 2016, 138, 14273−14287

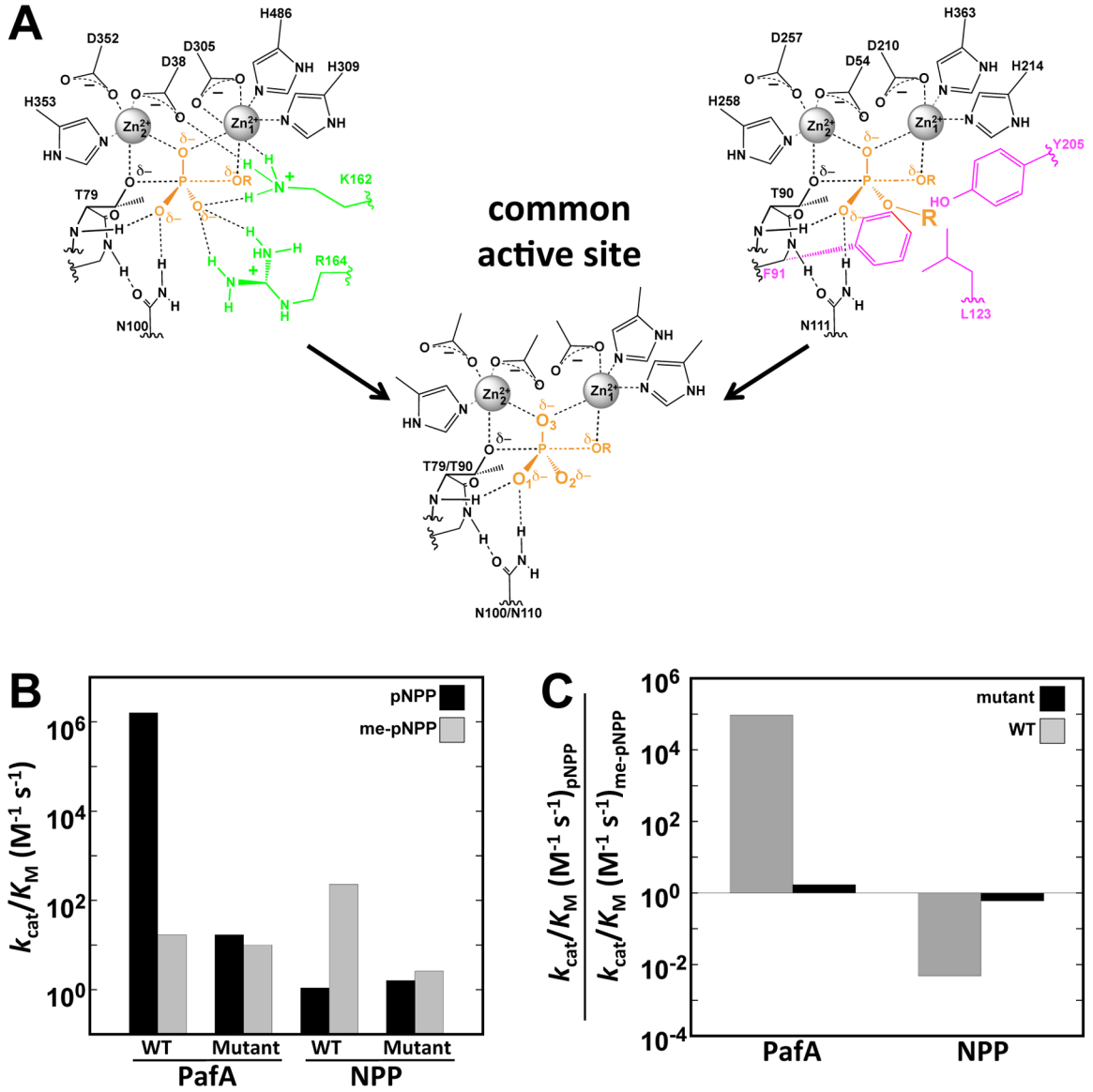

Figure 3. Comparative kinetics for wild-type and "common" PafA and NPP variants. (A) Schematics of the active residues in PafA (green) and NPP (magenta) that are removed to give mutants with common active-site residues. The residues removed interact with substrate oxygen O_2 in the PafA monoesterase reaction (Scheme 2) and the R′ group attached to this oxygen atom in the NPP diesterase reaction. (B) k_{cat}/K_M values for WT PafA, WT NPP, and the common core mutants. Phosphomonoester reactions are shown by black bars (pNPP) and phosphodiester reactions (me-pNPP) by gray bars. Rate constants are from Table 5. (C) The ratio of phosphomonoester to phosphodiester hydrolysis for WT PafA and WT NPP (gray) and for the common core mutants (black). The ratio of these ratios gives the relative specificity for the enzyme.

O_2 accepts hydrogen bonds from K162 and R164 (Figure 2). Correspondingly, mutation of N100 gives a uniform deleterious effect on monoester and diester hydrolysis, suggesting that this interaction facilitates both reactions, and mutations of K162 and R164 are deleterious only to phosphate monoester hydrolysis, with essentially no effect on the diester reaction (Figure 5A). Further, the opposite behavior is observed for NPP—i.e., mutations of the residues that constitute the R′ binding pocket are deleterious to NPP's diesterase activity but not to its monoesterase activity.[36]

The presence of distinct interactions with each of the two phosphoryl oxygen atoms or substituents in PafA and NPP allow interactions around one of the phosphoryl oxygen atoms to be altered and optimized for phosphate monoester or diester catalysis, while the interactions with the phosphoryl oxygen atom that contributes equally to both reactions can be maintained. We propose that the structural and functional modularity of the phosphoryl oxygen interactions facilitated evolutionary transitions between phosphate mono- and diesterases across the AP superfamily.[62] Information of this type about the functional architecture of active sites may also be powerful in guiding efforts to reengineer enzymes for new functions.

Beyond the O_2 and R′ Site in PafA and NPP: Extensive Sequence Variation in These Enzymes' Scaffolds Does Not Contribute to Reaction Specificity. The Zn^{2+} bimetallo site is a hallmark of a major branch of the AP superfamily and, as is generally the case for conserved features of superfamilies, is thought to play the same role across different reactions.[30,31] For the AP Zn^{2+} bimetallo site, one Zn^{2+} presumably deprotonates and positions the nucleophilic serine or threonine, the other Zn^{2+} stabilizes charge accumulation on the leaving group

DOI: 10.1021/jacs.6b06186
J. Am. Chem. Soc. 2016, 138, 14273−14287

Table 5. Comparison of Rate Constants for WT and Mutants of PafA and NPP[a]

	k_{cat}/K_M (M^{-1} s^{-1})			rate enhancement[d]	
enzyme	pNPP	me-pNPP	k_{rel}[c]	pNPP	me-pNPP
WT PafA	1.6(0.4) × 10^6	1.7(0.5) × 10^1	9.4 × 10^4	5.3 × 10^{16}	5.3 × 10^{12}
WT NPP[b]	1.1	230	4.8 × 10^{-3}	3.7 × 10^{10}	7.0 × 10^{13}
PafA K162A/R164A	16(6)	10(0.1)	1.6	5.3 × 10^{11}	3.0 × 10^{12}
NPP F91A/L123A/Y205A	1.6(0.1)	2.6(0.4)	0.6	5.3 × 10^{10}	7.9 × 10^{11}

[a]Assay conditions: 100 mM sodium MOPS, pH 8.0, 500 mM NaCl, 100 μM $ZnCl_2$. [b]Rate constants from ref 32. [c]Calculated as the ratio of $(k_{cat}/K_M)_{pNPP}/(k_{cat}/K_M)_{Me\text{-}pNPP}$. [d]Rate enhancements are calculated as $(k_{cat}/K_M)/k_W$ using the water hydrolysis rate constants of K_W^{pNPP} = 3.0 × 10^{-11} M^{-1} s^{-1} and $K_W^{Me\text{-}pNPP}$ = 3.3 × 10^{-12} M^{-1} s^{-1}.[65]

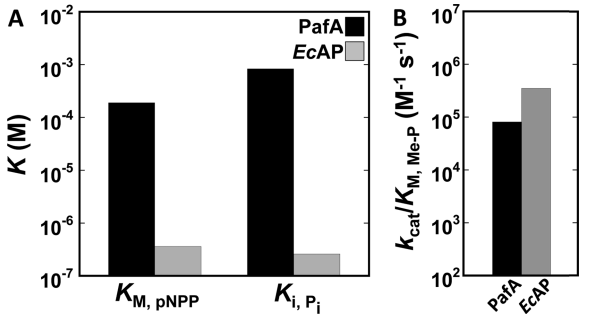

Figure 4. Comparison of *Ec*AP and PafA kinetics. (A) Values of K_M for phosphomonoester hydrolysis by WT PafA (black) and *Ec*AP (gray) and inhibition constants (K_i) for binding the product, inorganic phosphate (P_i). Values are from Tables 2 and 4 and refs 38 and 56. (B) k_{cat}/K_M values for phosphomonoester (Me-P) hydrolysis by WT PafA (black) and *Ec*AP (gray). Values are from Table 3 and ref 17.

oxygen atom, and there are also preferential interactions with the non-bridging oxygen atom that is situated between the Zn^{2+} ions in the transition state (Scheme 2).[65]

Nevertheless, the transition states for phosphate monoester and diester reactions differ in bond lengths and charge distributions, so the catalytic contributions from the Zn^{2+} interactions could differ quantitatively.[65] In particular, the different scaffolds surrounding the conserved Zn^{2+} ions and ligands could, in principle, adjust their positions or tune their charge densities to favor interactions with a phosphate monoester or diester transition state.[66] There is no structural evidence to support such differences,[66] but the differences could be small, transient, or only in electric field.

We therefore tested whether the PafA and NPP scaffolds, which differ in >80% of their residues (Supporting Information S5), provide functional specialization for each enzyme's cognate reaction. We created "common" mutant forms of PafA and NPP with the disparate residues interacting with the O_2 atom in PafA and the R′ group in NPP removed but the rest of the surrounding PafA and NPP scaffolds maintained (Figure 3A). Remarkably, whereas WT PafA and NPP differ in their preference for reaction with phosphate mono- and diesters by >10^7-fold, the mutant versions catalyze both reactions equally well (Figure 3B,C; the 10^7-fold difference in preference was calculated as the ratio of the ratios of the specificity for pNPP over me-pNPP for each enzyme in Figure 3C; see also ref 67). Thus, despite having evolved to carry out different cognate reactions and despite very low sequence identity, PafA and NPP have essentially identical specificities after removal of only five characteristic local active-site residues—three from NPP and two from PafA (Figure 3A). While this represents the simplest and most likely model, the possibility of secondary conformational rearrangements of either enzyme that co-incidentally lead to the same activity will require structural comparisons.

As the rate enhancements of these mutants are substantial (~10^{11}–10^{12}-fold) and rivaling enhancements observed for many fully evolved enzymes (Table 5),[68], and as the >10^7-fold difference in native specificities appears to arise from interactions at a single phosphoryl position, these scaffolds seem to provide excellent jumping off points for evolving or engineering highly efficient and specific phosphate monoesterases and diesterases.

Comparisons across the AP Superfamily Suggest Active-Site Roles for Specific Structural Elements. As emphasized in the Introduction, understanding enzyme function will require the identification of structural connections beyond the active site. Indeed, the notion that the enzyme scaffold positions binding and catalytic groups for catalysis is the fundamental precept of enzymology (e.g., refs 69–72). While the importance of elements beyond the active site is

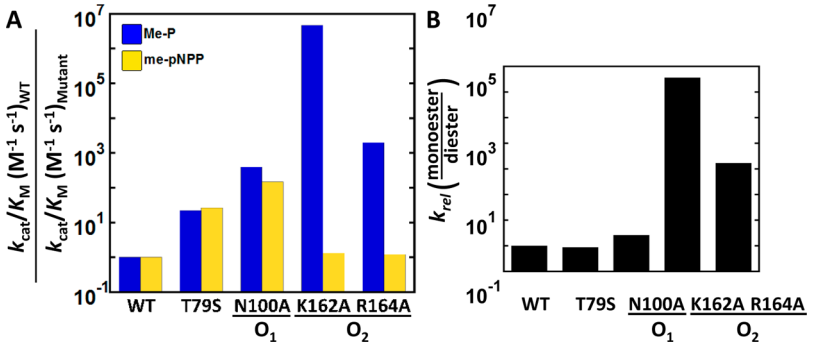

Figure 5. Effect of PafA mutations on phosphate monoester and diester hydrolysis. (A) Ratio of k_{cat}/K_M values for PafA mutants for phosphomonoester (blue) and phosphodiester (yellow) reactions. Reactions are for Me-P and me-pNPP (Chart 1), and kinetic values are from Tables 2 and 3. (B) Ratio of the mutational effects on the phosphate monoester and diester reactions, with larger values representing larger effects on the monoester relative to diester reaction. The phosphoryl oxygen atom (Scheme 2) that each residue interacts with is noted and is based on the structural schematic of Figure 2.

DOI: 10.1021/jacs.6b06186
J. Am. Chem. Soc. 2016, 138, 14273–14287

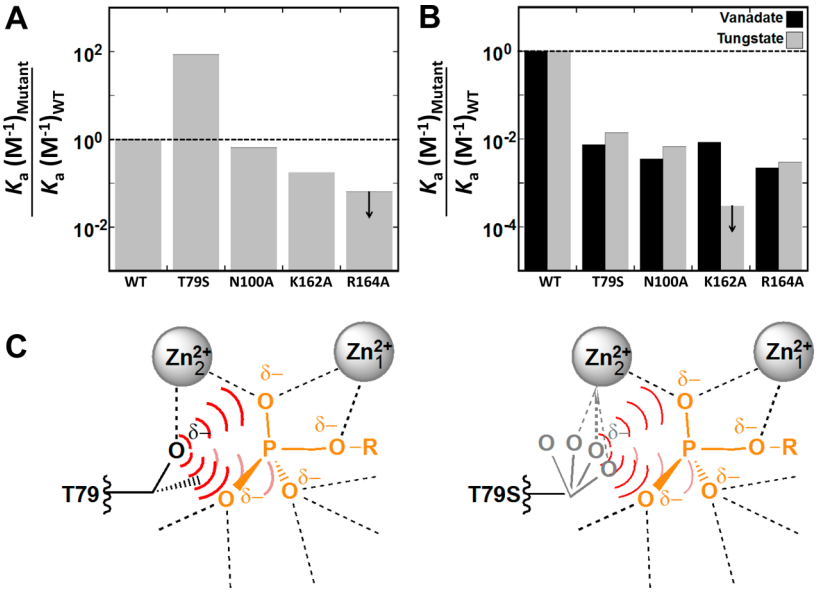

Figure 6. Evidence for electrostatic ground-state destabilization. (A) Ratio of affinities (K_a) for binding of the ground-state analogue P_i to PafA active-site mutants, relative to WT PafA. The dashed line represents a ratio of one, the value for WT PafA by definition. The arrow for R164A indicates an upper limit. Data are from Table 4. (B) Ratio of affinities (K_a) for binding of putative transition-state analogues vanadate (black) and tungstate (gray) to PafA active-site mutants, relative to WT PafA. The dashed line represents a ratio of one, the value for WT PafA by definition. The arrow for K162A indicates an upper limit. Data are from Table 4. (C) Model for electrostatic ground-state destabilization in WT PafA that is partially relieved in the T79S mutant due to lessened conformational restriction of the oxyanion of this residue. This model predicts lowered reactivity, weakened binding of transition-state analogues, and stronger binding of a ground-state analogue, as is observed. Only the T79S mutation exhibits this set of effects.

clear, identifying their roles has been difficult. For example, most attempts to convert one enzyme to another start from highly related enzymes with a finite set of amino acid differences and have used trial-and-error strategies,[73−75] and engineering efforts have generally not reproduced natural catalytic efficiencies.[76−80] Here, comparisons across the AP superfamily allowed us to identify two structural elements that may make specific functional connections to the active site.

As emphasized above, PafA and NPP catalyze distinct reactions but have common interactions with phosphoryl oxygen atom O_1 (Figures 2 and 3A). Strikingly, PafA and NPP share an inserted structural element that is not present in *Ec*AP, which catalyzes the same reaction as PafA but has distinct O_1 interactions. This insertion is situated between conserved sheets 6 and 7 in PafA and NPP and sits directly behind the common asparagine residue in their three-dimensional structures (Figure 1B and Supporting Information S7). Given this observation, we surveyed all 27 bimetallo AP superfamily members for which high-resolution structures are available. Of these, 10 contained a residue homologous to N100 of PafA and N111 of NPP, and in all cases these enzymes also contained an insertion at the position observed for PafA and NPP. Further, none of the enzymes lacking a corresponding asparagine contained this insertion (Supporting Information S8, Table 1). This correspondence suggests that the inserted structural elements play a common role in positioning the active-site asparagine for its interactions with an oxygen O_1 of the transferred phosphoryl group (Figures 1 and 2).

There is also evidence for a helical element that may govern phosphate monoesterase activity. PafA and *Ec*AP contain a helix (4a) that is inserted after β sheet 3 and is absent in NPP (Figure 1B; Supporting Information S9). Within or adjoining this helix are residues interacting with O_2 in PafA (K162 and R164) and *Ec*AP (D153) as well as the *Ec*AP Mg^{2+} ligand T155 (Figures 1B and 2). Repeating the above structural analysis revealed that helix 4a is present in all structurally characterized AP superfamily members that catalyze reactions of monosubstituted phosphates and is absent in all members that catalyze reactions of phosphate diesters (Supporting Information S8, Table 1). Additional elements accompany the helix 4a insertion (e.g., helices 4a-e and β sheet 4a for PafA; helices 4a-g, and β sheet 4a-b for *Ec*AP; Figure 1B) but are absent in the diesterases, perhaps because their role is to position helix 4a and the nearby active-site residues, akin to the structural elements behind the conserved asparagine of PafA and NPP described above. Thus, helix 4a and the remainder of this monoester-specific insert may help position active-site residues for interactions with O_2 of monosubstituted phosphate substrates.

The absence of the 4a helix in diesterases could reflect the absence of selective pressure to maintain it, or it could be selected against to provide space for a bulky diester substituent on O_2 and allow a more remote binding site to be sculpted for that substituent. Most generally, understanding whether active-site elements work cooperatively with adjacent structural elements or distinctly will help elucidate the evolutionary history of enzymes within and beyond the AP superfamily and may also suggest effective modular approaches to the problem of engineering new enzymes.

Mechanistic Commonalities between EcAP and PafA Phosphate Monoesterases. For catalysis to occur, an enzyme must stabilize a reaction's transition state to a greater extent than the reaction's ground state; otherwise, if both are stabilized to the same extent, the reaction barrier is the same on the enzyme as off of the enzyme so that there is no catalysis.[81−85] In essence, such destabilization occurs in all enzymatic reactions, as fixation of reactants in the active site can be considered as entropically destabilizing, even though

DOI: 10.1021/jacs.6b06186
J. Am. Chem. Soc. 2016, 138, 14273−14287

quantification of this destabilization has proven elusive. Prior experiments with *Ec*AP showed that P_i binds orders of magnitude stronger to *Ec*AP mutants when the anionic serine residue is removed. These and additional data provided strong evidence for electrostatic ground-state destabilization and a quantitative estimate of at least 10^3-fold for this effect.[56,57]

Our results with PafA suggest that its active site harnesses analogous ground-state destabilization. Mutation of the nucleophilic threonine to serine decreases catalysis and weakens binding to vanadate and tungstate transition-state analogues[86,87] by ∼100-fold (Figure 6B), similar to the ∼20-fold decrease in activity (Figure 5) as expected for transition-state analogues (see also Discrimination between Transition-State Analogues in AP Superfamily Active Sites Suggests Precise Transition-State Recognition, below). But in contrast, this mutation *increases* inhibition by P_i by >100-fold (Figure 6A, Table 4).

These effects are predicted from the ground-state electrostatic destabilization model shown in Figure 6C. The decreased activity and decreased transition-state analogue binding are predicted from loosening the positioning of the nucleophilic oxyanion, resulting from a loss of interactions with the methyl group of T79. The reaction and formation of covalent vanadate and tungstate adducts now requires overcoming an additional barrier for proper positioning and are correspondingly less favorable. In contrast, greater freedom of motion of the seryl oxyanion (Figure 6C, right) allows it to move away from anionic phosphate ligand, thereby lessening electrostatic repulsion and allowing the observed increase in P_i binding. The 80-fold stronger binding corresponds to 2.2 kcal/mol of destabilization energy, providing a lower limit for the extent of ground-state destabilization, as some destabilization may remain in the mutant.[88]

Interestingly, while *Ec*AP and PafA both appear to utilize electrostatic ground-state destabilization to facilitate catalysis, the interactions that are responsible for positioning the oxyanion for nucleophilic attack and providing ground-state repulsion differ for the two enzymes. *Ec*AP has a nucleophilic serine and so lacks the methyl group of PafA's threonine residue that contributes to oxyanion positioning. Understanding the strategies used to position the threonyl and seryl nucleophiles will help uncover distinct evolutionary solutions to a common problem and may help reveal the types and extent of interactions needed to efficiently engineer new enzymes.

Another functional analogy between PafA and *Ec*AP that involves distinct interactions was suggested from our mutagenesis results. Prior results revealed a ∼10^5-fold rate decrease from removal of the active-site Mg^{2+} of *Ec*AP (via mutation of one of its ligands, E322; Figure 2)[24] and showed that this Mg^{2+} ion acts as part of a functional network with K328, D153, and a set of bound water molecules (Figure 7A, blue).[17,24] Such a large effect is rare for a group not directly involved in chemical catalysis (like the serine nucleophile) and implies important functional role of this interaction network. Thus, it was particularly noteworthy to observe a 10^6-fold rate decrease in phosphate monoester catalysis upon mutation of K162 (Figure 5A), a residue that has no direct role in PafA's reaction chemistry (Figure 2) and, similar to the observation of *Ec*AP's Mg^{2+} removal, had little effect on PafA's diesterase activity (Figure 5A).

Intriguingly, although there is no structural homology or sequence identity in this region of PafA and *Ec*AP, analogous interaction networks can be drawn for K162 of PafA and the Mg^{2+} ion of *Ec*AP (Figure 7). In PafA (Figure 7B), K162 donates a hydrogen bond to the O_2 phosphoryl oxygen atom, like the $Mg^{2+}{\cdot}OH_2$ of *Ec*AP (Figure 7A). K162 also hydrogen bonds to D38, the residue homologous to D51 of *Ec*AP that is also a Mg^{2+} ligand. In addition, K162 hydrogen bonds to D305, the Zn_1 ligand that is homologous to D327 of *Ec*AP.

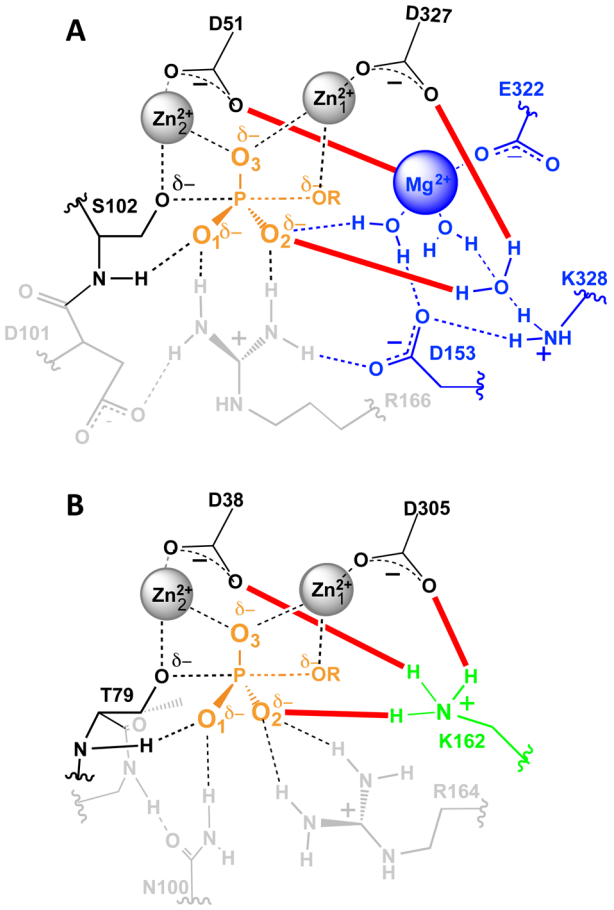

Figure 7. Analogous hydrogen bond networks in PafA (A) and *Ec*AP (B). Each active-site schematic highlights a hydrogen bond network, that involving the active-site Mg^{2+} of *Ec*AP and its associated network (A, blue) or K162 of PafA (B, green). The red lines highlight the analogous interactions made with other active-site elements. The common conserved Zn^{2+} bimetallo sites, including the serine or threonine nucleophile, are shown in black, and other active-site residues are shown in gray.

Given the remarkable correspondence of active-site connections and similar large functional effects, the Mg^{2+} ion of *Ec*AP and K162 of PafA may play analogous important functional roles and may represent distinct evolutionary solutions to analogous structural and functional challenges within AP superfamily active sites. Structural inspection suggests that these groups make connections within the active site that may simultaneously optimize the position of the two Zn^{2+} ions, the threonine or serine nucleophile, and the transferred phosphoryl group, via one of its non-bridging oxygen atoms (Figure 7). These observations may help define the type and degree of interconnections that are needed to engineer and re-engineer highly efficient enzymes.

Discrimination between Transition-State Analogues in AP Superfamily Active Sites Suggests Precise Transition-State Recognition. A recent high-resolution crystal structure of WT *Ec*AP revealed that tungstate, like

DOI: 10.1021/jacs.6b06186
J. Am. Chem. Soc. 2016, 138, 14273−14287

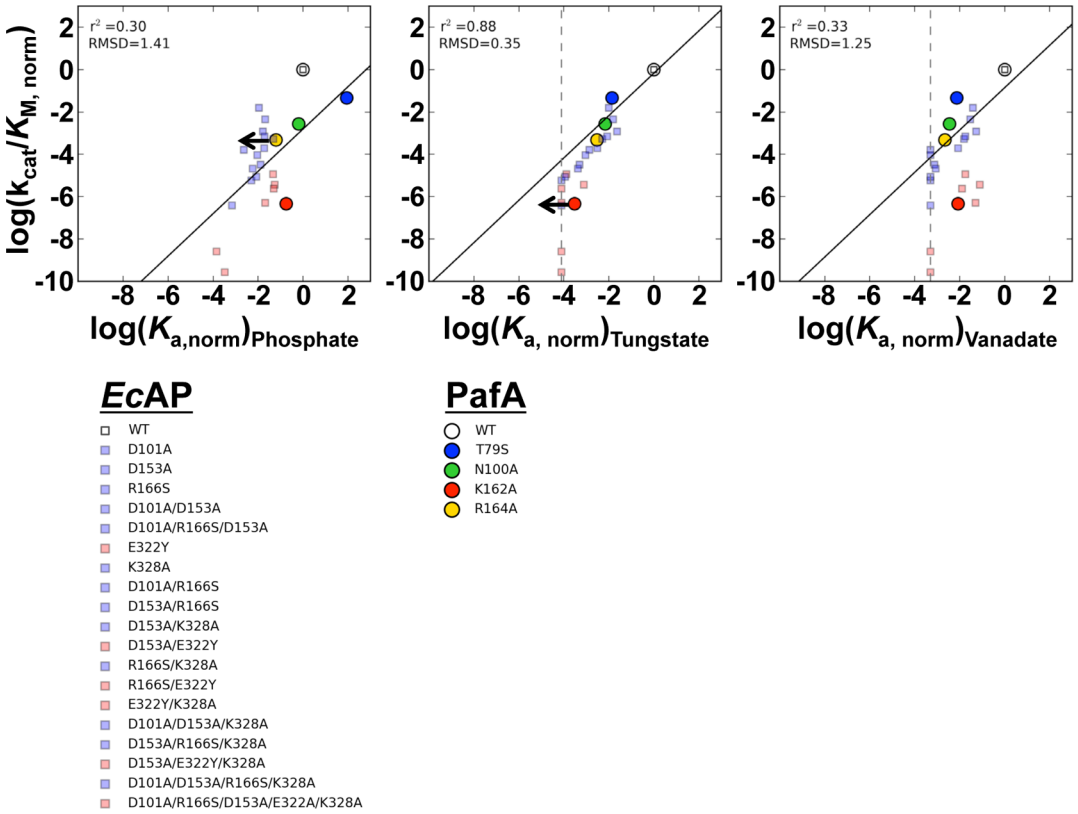

Figure 8. Correlation of activity and affinity for ground- and transition-state analogues. Correlations of activity values (k_{cat}/K_M measured with Me-P normalized to WT PafA, and k_{cat}/K_M measured with pNPP normalized to WT *Ec*AP) with inhibition ($K_a = 1/K_i$) by inorganic phosphate (P_i), tungstate, and vanadate. Data for PafA (circles) from Table 3 [$(k_{cat}/K_M)_{Me\text{-}P}$] and Table 4; data for *Ec*AP (light squares) from ref 87. The solid lines are fits to the PafA data with fixed slopes of 1, as expected for a transition-state analogue;[89,90] the rmsd given is for deviation from these lines; and Pearson's R^2 values are also listed. Statistical tests were carried out as described by Peck et al.,[87] and additional statistical parameters for PafA and *Ec*AP are given in Table 6. Values at the vertical dashed lines marked with arrows represent lower limits for affinity for AP variants and were not included in the fits. Similarly PafA points that are limits are denoted with an arrow and were excluded from fitting of the data. The PafA mutants are color-coded as noted in the attached legend. The *Ec*AP mutants are specified and color-coded as follows: WT, white; mutants with the Mg^{2+} ion removed (E322Y or E322A), red; all other mutants, blue; these data represent combinations of mutations at five active-site residues, and the individual data points can be found in ref 87.

vanadate, binds as a covalent pentavalent adduct, mimicking the reaction's transition-state geometry.[87] Extensive analysis of the catalytic properties of 20 *Ec*AP variants relative to the binding of P_i, vanadate, and tungstate showed that tungstate binding mirrors activity much more closely than P_i binding and also more closely than vanadate binding.[87] Thus, tungstate meets the most stringent criterion for acting as a transition-state analogue, although no stable analogue can perfectly mimic a transient, partially bonded transition state.[89]

We also see a better correlation of activity and binding for tungstate for the five PafA variants studied herein (Figure 8). Tungstate gives a higher coefficient of determination (Pearson R^2) than vanadate and P_i and a best-fit slope closer to one (Table 6), as expected for a transition-state analogue.[89,90] Similarly, when the correlation slope is fixed at one (Figure 8), the RMSD is considerably lower for tungstate than vanadate or P_i (Table 6). Figure 8 and Table 6 include the results for *Ec*AP (semi-transparent squares), highlighting that tungstate more closely mimics the behavior expected for a transition-state analogue with both *Ec*AP and PafA.

We noted previously that a subset of *Ec*AP variants—mutants that removed the active-site Mg^{2+} ion addressed in the preceding section—were predominantly responsible for the poorer correlation of binding and activity for vanadate than tungstate (Figure 8, red squares).[87] Intriguingly, for PafA, the K162 mutant deviated substantially with vanadate but fell closer to the line with tungstate (Figure 8, red circles, the tungstate value is a limit). This result extends the analogy between K162 of PafA and the active-site Mg^{2+} ion of *Ec*AP (Figure 7) and suggests a high degree of precision to discriminate between tungstate and vanadate species within the active site of these extremely efficient enzymes.

Table 6. Statistical Test for Transition Analog Behavior.[a]

		phosphate		tungstate		vanadate	
		PafA	*Ec*AP	PafA	*Ec*AP	PafA	*Ec*AP
Pearson's r^2		0.54	0.74	0.94	0.94	0.57	0.48
orthogonal distance regression	m[b]	3.8	3.3	1.3	1.4	3.4	3.8
	rmsd[c]	0.82	0.54	0.28	0.28	0.75	0.66
constrained regression (m = 1)	rmsd[c]	1.41	1.15	0.35	0.41	1.25	1.04

[a]Analysis of data presented in Figure 8. [b]Slope of best fit line determined from orthogonal distance regression. [c]Root-mean-squared deviation (RMSD) calculated from the orthogonal distances between data points and the linear fit with either a variable slope (m) or a slope fixed at m = 1.

DOI: 10.1021/jacs.6b06186
J. Am. Chem. Soc. 2016, 138, 14273−14287

GENERAL IMPLICATIONS

Over the past decades, there has been an enormous amount learned about how enzymes catalyze reactions, in terms of the underlying chemical mechanisms, the residues and cofactors that facilitate those reactions, and the overall structural context in which these reactions take place. Nevertheless, there is also an enormous amount that we do not yet understand, as exemplified by the limited ability to engineer new enzymes and the prevalence of trial-and-error approaches.

Given that we can identify the residues directly involved in binding and catalysis, the next stage of understanding will entail deciphering how protein scaffolds and interaction networks assemble and position active-site residues for catalysis. Enzyme superfamilies provide sets of enzymes with functional distinctions in similar overall structural contexts,[91,92] and catalytic promiscuity provides a means to probe the functional consequences of the structural elements and sequence features that differ between superfamily members.[24] Thus, superfamily members provide sufficient "contrast" to make meaningful comparisons, but sufficient similarities to allow inferences to be drawn from their juxtaposition, and catalytic promiscuity allows systematic and multi-dimensional functional analysis across superfamily members and properties.

Propitiously, enzymes of the AP superfamily have been highly amenable to comparative approaches (e.g., refs 32, 35, 93, and 94). We have taken advantage of the occurrence of distinct AP superfamily phosphate monoesterases, one of which has features similar to the superfamily diesterases that are absent in another monoesterase (Figures 1 and 2). Multi-faceted comparisons of structure, sequence, and cognate and promiscuous reactions of these superfamily members and their mutants in this work and previously have extended our mechanistic understanding, have led to models for the roles of active site and more distal structural elements, and have suggested evolutionary driving forces and adaptations.[17,24,32,34−36,38,51,52,56,58,59,87,95−98]

While this work represents modest steps toward a deeper and more comprehensive understanding of enzyme assembly and function, we are heartened by how many insights have arisen by making comparisons across superfamilies of cognate and promiscuous reactions. This approach to a mechanistic puzzle might be likened, abstractly, to an algebraic problem. In algebra one needs the number of equations to at least match the number of variables; for the complex problem of enzyme mechanism, we require a large number of comparisons. In addition, as in algebra where the equations used need to be orthogonal to one another, different types of comparisons are needed to assess different aspects of mechanism. Structural, sequence, and functional comparisons of superfamily members, in conjunction with comparisons of cognate and promiscuous activities, provide complementary and powerful approaches toward the goal of understanding the features and factors responsible for assembly of an enzyme and for its catalytic function. While this enormously complex problem will undoubtedly require many studies and the development of new approaches, the partial structural and functional modularity suggested herein and by prior results[17] may simplify the path to the robust engineering of novel, highly effective enzymes.

ASSOCIATED CONTENT

Supporting Information

The Supporting Information is available free of charge on the ACS Publications website at DOI: 10.1021/jacs.6b06186.

S1, PafA gene sequence; S2, pH dependencies for PafA WT and mutants; S3, inhibition curves for PafA WT and mutants; S4, determination of Me-P kinetics at pH 8; S5−S9, sequence alignments and structural comparisons in the AP superfamily (PDF)

Crystallographic data for PafA_refine_reflections (CIF)

Crystallographic data for PafA_refine_99 (CIF)

AUTHOR INFORMATION

Corresponding Author

*herschla@stanford.edu

Notes

The authors declare no competing financial interest.

ACKNOWLEDGMENTS

This work was funded by a grant from the U.S. National Institutes of Health to D.H. (GM49243); partial support for J.B., C.L.B., and Z.S. was provided by National Science Foundation grant (MCB-1121778). J.B. was an Amgen Scholar in the Stanford Summer Research Program, and C.B. was a Stanford ADVANCE Institute fellow. The SSRL Structural Molecular Biology Program is supported by the Department of Energy, Office of Biological and Environmental Research, and by the National Institutes of Health, National Center for Research Resources, Biomedical Technology Program, and the National Institute of General Medical Sciences. We thank Emily Burnette for technical assistance, Axel Brunger for support, and Monarin Uervirojnangkoorn in the Brunger laboratory for discussion and advice on the diffraction data processing and structure refinement. We thank Patricia Babbitt, and Gemma Holliday and members of the Babbitt laboratory for discussions on phylogeny. We thank Jonathan Lassila, Craig Markin, and Ariana Peck for discussions about structural and energetic aspects of this work. We thank members of the Herschlag laboratory for discussions and comments on the manuscript.

REFERENCES

(1) Kraut, D. A.; Carroll, K. S.; Herschlag, D. *Annu. Rev. Biochem.* **2003**, *72*, 517.

(2) Herschlag, D.; Natarajan, A. *Biochemistry* **2013**, *52*, 2050.

(3) Horovitz, A. *Folding Des.* **1996**, *1*, R121.

(4) Singh, P.; Sen, A.; Francis, K.; Kohen, A. *J. Am. Chem. Soc.* **2014**, *136*, 2575.

(5) Narlikar, G. J.; Herschlag, D. *Biochemistry* **1998**, *37*, 9902.

(6) Carter, P. J.; Winter, G.; Wilkinson, A. J.; Fersht, A. R. *Cell* **1984**, *38*, 835.

(7) Hermes, J. D.; Blacklow, S. C.; Knowles, J. R. *Proc. Natl. Acad. Sci. U. S. A.* **1990**, *87*, 696.

(8) Horovitz, A.; Bochkareva, E. S.; Yifrach, O.; Girshovich, A. S. *J. Mol. Biol.* **1994**, *238*, 133.

(9) Masterson, L. R.; Mascioni, A.; Traaseth, N. J.; Taylor, S. S.; Veglia, G. *Proc. Natl. Acad. Sci. U. S. A.* **2008**, *105*, 506.

(10) Freedman, T. S.; Sondermann, H.; Kuchment, O.; Friedland, G. D.; Kortemme, T.; Kuriyan, J. *Structure* **2009**, *17*, 41.

(11) Rajagopalan, S.; Lutz, S.; Benkovic, S. J. *Biochemistry* **2002**, *41*, 12618.

(12) Dion, A.; Linn, C. E.; Bradrick, T. D.; Georghiou, S.; Howell, E. E. *Biochemistry* **1993**, *32*, 3479.

(13) Lockless, S. W.; Ranganathan, R. *Science* **1999**, *286*, 295.

DOI: 10.1021/jacs.6b06186
J. Am. Chem. Soc. 2016, 138, 14273−14287

(14) Doucet, N.; Khirich, G.; Kovrigin, E. L.; Loria, J. P. *Biochemistry* **2011**, *50*, 1723.
(15) Halabi, N.; Rivoire, O.; Leibler, S.; Ranganathan, R. *Cell* **2009**, *138*, 774.
(16) Eisenmesser, E. Z.; Millet, O.; Labeikovsky, W.; Korzhnev, D. M.; Wolf-Watz, M.; Bosco, D. A.; Skalicky, J. J.; Kay, L. E.; Kern, D. *Nature* **2005**, *438*, 117.
(17) Sunden, F.; Peck, A.; Salzman, J.; Ressl, S.; Herschlag, D. *eLife* **2015**, *4*, e06181.
(18) Gerlt, J. A.; Allen, K. N.; Almo, S. C.; Armstrong, R. N.; Babbitt, P. C.; Cronan, J. E.; Dunaway-Mariano, D.; Imker, H. J.; Jacobson, M. P.; Minor, W.; Poulter, C. D.; Raushel, F. M.; Sali, A.; Shoichet, B. K.; Sweedler, J. V. *Biochemistry* **2011**, *50*, 9950.
(19) Gerlt, J. A.; Babbitt, P. C.; Rayment, I. *Arch. Biochem. Biophys.* **2005**, *433*, 59.
(20) Meng, Q.; Chen, K.; Ma, L.; Hu, S.; Yu, J. *J. Genet. Genomics* **2011**, *38*, 63.
(21) Jensen, R. A. *Annu. Rev. Microbiol.* **1976**, *30*, 409.
(22) O'Brien, P. J.; Herschlag, D. *Chem. Biol.* **1999**, *6*, R91.
(23) Khersonsky, O.; Tawfik, D. S. *Annu. Rev. Biochem.* **2010**, *79*, 471.
(24) Zalatan, J. G.; Fenn, T. D.; Herschlag, D. *J. Mol. Biol.* **2008**, *384*, 1174.
(25) van Loo, B.; Jonas, S.; Babtie, A. C.; Benjdia, A.; Berteau, O.; Hyvonen, M.; Hollfelder, F. *Proc. Natl. Acad. Sci. U. S. A.* **2010**, *107*, 2740.
(26) Kim, A.; Benning, M. M.; OkLee, S.; Quinn, J.; Martin, B. M.; Holden, H. M.; Dunaway-Mariano, D. *Biochemistry* **2011**, *50*, 3481.
(27) Jonas, S.; van Loo, B.; Hyvonen, M.; Hollfelder, F. *J. Mol. Biol.* **2008**, *384*, 120.
(28) Gijsbers, R.; Ceulemans, H.; Stalmans, W.; Bollen, M. *J. Biol. Chem.* **2001**, *276*, 1361.
(29) Chapman, E.; Best, M. D.; Hanson, S. R.; Wong, C. H. *Angew. Chem., Int. Ed.* **2004**, *43*, 3526.
(30) Galperin, M. Y.; Bairoch, A.; Koonin, E. V. *Protein Sci.* **1998**, *7*, 1829.
(31) Galperin, M. Y.; Jedrzejas, M. J. *Proteins: Struct., Funct., Genet.* **2001**, *45*, 318.
(32) Zalatan, J. G.; Fenn, T. D.; Brunger, A. T.; Herschlag, D. *Biochemistry* **2006**, *45*, 9788.
(33) Olguin, L. F.; Askew, S. E.; O'Donoghue, A. C.; Hollfelder, F. *J. Am. Chem. Soc.* **2008**, *130*, 16547.
(34) O'Brien, P. J.; Lassila, J. K.; Fenn, T. D.; Zalatan, J. G.; Herschlag, D. *Biochemistry* **2008**, *47*, 7663.
(35) Lassila, J. K.; Herschlag, D. *Biochemistry* **2008**, *47*, 12853.
(36) Wiersma-Koch, H. I.; Sunden, F.; Herschlag, D. *Biochemistry* **2013**, *52*, 9167.
(37) Lanzetta, P. A.; Alvarez, L. J.; Reinach, P. S.; Candia, O. A. *Anal. Biochem.* **1979**, *100*, 95.
(38) O'Brien, P. J.; Herschlag, D. *Biochemistry* **2002**, *41*, 3207.
(39) Battye, T. G.; Kontogiannis, L.; Johnson, O.; Powell, H. R.; Leslie, A. G. *Acta Crystallogr., Sect. D: Biol. Crystallogr.* **2011**, *67*, 271.
(40) Powell, H. R.; Johnson, O.; Leslie, A. G. *Acta Crystallogr., Sect. D: Biol. Crystallogr.* **2013**, *69*, 1195.
(41) Evans, P. *Acta Crystallogr., Sect. D: Biol. Crystallogr.* **2006**, *62*, 72.
(42) Padilla, J. E.; Yeates, T. O. *Acta Crystallogr., Sect. D: Biol. Crystallogr.* **2003**, *59*, 1124.
(43) McCoy, A. J.; Grosse-Kunstleve, R. W.; Adams, P. D.; Winn, M. D.; Storoni, L. C.; Read, R. J. *J. Appl. Crystallogr.* **2007**, *40*, 658.
(44) McCoy, A. J. *Acta Crystallogr., Sect. D: Biol. Crystallogr.* **2007**, *63*, 32.
(45) Emsley, P.; Lohkamp, B.; Scott, W. G.; Cowtan, K. *Acta Crystallogr., Sect. D: Biol. Crystallogr.* **2010**, *66*, 486.
(46) Adams, P. D.; et al. *Acta Crystallogr., Sect. D: Biol. Crystallogr.* **2010**, *66*, 213.
(47) Urzhumtseva, L.; Afonine, P. V.; Adams, P. D.; Urzhumtsev, A. *Acta Crystallogr., Sect. D: Biol. Crystallogr.* **2009**, *65*, 297.
(48) Murshudov, G. N. *Appl. Comput. Math.* **2011**, *10*, 250.
(49) Chen, V. B.; Arendall, W. B., 3rd; Headd, J. J.; Keedy, D. A.; Immormino, R. M.; Kapral, G. J.; Murray, L. W.; Richardson, J. S.; Richardson, D. C. *Acta Crystallogr., Sect. D: Biol. Crystallogr.* **2010**, *66*, 12.
(50) Pettersen, E. F.; Goddard, T. D.; Huang, C. C.; Couch, G. S.; Greenblatt, D. M.; Meng, E. C.; Ferrin, T. E. *J. Comput. Chem.* **2004**, *25*, 1605.
(51) Bihani, S. C.; Das, A.; Nilgiriwala, K. S.; Prashar, V.; Pirocchi, M.; Apte, S. K.; Ferrer, J.; Hosur, M. V. *PLoS One* **2011**, *6*, e22767.
(52) Berlutti, F.; Passariello, C.; Selan, L.; Thaller, M. C.; Rossolini, G. M. *Microbiology* **2001**, *147*, 2831.
(53) Nilgiriwala, K. S.; Bihani, S. C.; Das, A.; Prashar, V.; Kumar, M.; Ferrer, J. L.; Apte, S. K.; Hosur, M. V. *Acta Crystallogr., Sect. F: Struct. Biol. Cryst. Commun.* **2009**, *65*, 917.
(54) Goding, J. W.; Grobben, B.; Slegers, H. *Biochim. Biophys. Acta, Mol. Basis Dis.* **2003**, *1638*, 1.
(55) Fersht, A. *Structure and mechanism in protein science. A guide to enzyme catalysis and protein folding*; W. H. Freeman and Co.: New York, 1999.
(56) Andrews, L. D.; Fenn, T. D.; Herschlag, D. *PLoS Biol.* **2013**, *11*, e1001599.
(57) Andrews, L. D.; Deng, H.; Herschlag, D. *J. Am. Chem. Soc.* **2011**, *133*, 11621.
(58) O'Brien, P. J.; Herschlag, D. *J. Am. Chem. Soc.* **1998**, *120*, 12369.
(59) O'Brien, P. J.; Herschlag, D. *Biochemistry* **2001**, *40*, 5691.
(60) Members of the AP superfamily branched very early in evolution, and their extreme diversity prevents establishment of a high-confidence rooted evolutionary tree. Without discovery of additional relevant sequences and determination of more three-dimensional structures to guide the multiple alignments required, we cannot determine whether the PafA- and NPP-like AP superfamily members originated from a monoesterase, diesterase, or generalist-like ancestor (P. C. Babbitt, personal communication).
(61) Ratner, H. *IC, Infect. Control* **1984**, *5*, 237.
(62) Santos-Beneit, F. *Front. Microbiol.* **2015**, *6*, 402.
(63) Kulakovskaya, T. V.; Lichko, L. P.; Ryazanova, L. P. *Biochemistry* **2014**, *79*, 1602.
(64) Me-P reactions are compared rather than reactions of pNPP, as the unactivated leaving group is more likely to mimic physiological substrates.
(65) Lassila, J. K.; Zalatan, J. G.; Herschlag, D. *Annu. Rev. Biochem.* **2011**, *80*, 669.
(66) Mildvan, A. S. *Proteins: Struct., Funct., Genet.* **1997**, *29*, 401.
(67) The specificity difference is larger with substrates that more closely resemble naturally occurring phosphate diesters and with substrates for which the chemical step is rate limiting (see Experimental Section and refs 32 and 38).
(68) Wolfenden, R.; Snider, M. J. *Acc. Chem. Res.* **2001**, *34*, 938.
(69) Narlikar, G. J.; Herschlag, D. *Annu. Rev. Biochem.* **1997**, *66*, 19.
(70) Blow, D. *Structure* **2000**, *8*, R77.
(71) Zastrow, M. L.; Pecoraro, V. L. *Biochemistry* **2014**, *53*, 957.
(72) Malashkevich, V. N.; Onuffer, J. J.; Kirsch, J. F.; Jansonius, J. N. *Nat. Struct. Biol.* **1995**, *2*, 548.
(73) Onuffer, J. J.; Kirsch, J. F. *Protein Sci.* **1995**, *4*, 1750.
(74) Cronin, C. N.; Malcolm, B. A.; Kirsch, J. F. *J. Am. Chem. Soc.* **1987**, *109*, 2222.
(75) Khersonsky, O.; Kiss, G.; Röthlisberger, D.; Dym, O.; Albeck, S.; Houk, K. N.; Baker, D.; Tawfik, D. S. *Proc. Natl. Acad. Sci. U. S. A.* **2012**, *109*, 10358.
(76) Korendovych, I. V.; DeGrado, W. F. *Curr. Opin. Struct. Biol.* **2014**, *27*, 113.
(77) Kiss, G.; Çelebi-Ölçüm, N.; Moretti, R.; Baker, D.; Houk, K. N. *Angew. Chem., Int. Ed.* **2013**, *52*, 5700.
(78) Althoff, E. A.; Wang, L.; Jiang, L.; Giger, L.; Lassila, J. K.; Wang, Z.; Smith, M.; Hari, S.; Kast, P.; Herschlag, D.; Hilvert, D.; Baker, D. *Protein Sci.* **2012**, *21*, 717.
(79) Lassila, J. K.; Baker, D.; Herschlag, D. *Proc. Natl. Acad. Sci. U. S. A.* **2010**, *107*, 4937.
(80) Baker, D. *Protein Sci.* **2010**, *19*, 1817.

DOI: 10.1021/jacs.6b06186
J. Am. Chem. Soc. 2016, 138, 14273−14287

(81) Jencks, W. P. *Cold Spring Harbor Symp. Quant. Biol.* **1987**, *52*, 65.
(82) Jencks, W. P. *Adv. Enzymol. Relat. Areas Mol. Biol.* **2006**, *43*, 219.
(83) Page, M. I.; Jencks, W. P. *Proc. Natl. Acad. Sci. U. S. A.* **1971**, *68*, 1678.
(84) Jencks, W. P. *Proc. Natl. Acad. Sci. U. S. A.* **1981**, *78*, 4046.
(85) Jencks, W. P.; Page, M. I. *Biochem. Biophys. Res. Commun.* **1974**, *57*, 887.
(86) Holtz, K. M.; Stec, B.; Kantrowitz, E. R. *J. Biol. Chem.* **1999**, *274*, 8351.
(87) Peck, A.; Sunden, F.; Andrews, L. D.; Pande, V. S.; Herschlag, D. *J. Mol. Biol.* **2016**, *428*, 2758.
(88) For EcAP, it has been shown that Pi binds in its fully deprotonated trianionic form, with the simultaneous uptake of a proton to neutralize the serine nucleophile (ref 56). This same binding presumably occurs with PafA. The stronger binding to the PafA T79S mutant is consistent with greater freedom of motion relieving remaining repulsion with the lone pair electrons of this oxygen atom at this position and/or a higher proton affinity from movement away from the Zn2 ion.
(89) Mader, M. M.; Bartlett, P. A. *Chem. Rev.* **1997**, *97*, 1281.
(90) Wolfenden, R. *Annu. Rev. Biophys. Bioeng.* **1976**, *5*, 271.
(91) Glasner, M. E.; Gerlt, J. A.; Babbitt, P. C. *Curr. Opin. Chem. Biol.* **2006**, *10*, 492.
(92) Gerlt, J. A.; Babbitt, P. C. *Annu. Rev. Biochem.* **2001**, *70*, 209.
(93) Mohamed, M. F.; Hollfelder, F. E. *Biochim. Biophys. Acta, Proteins Proteomics* **2013**, *1834*, 417.
(94) Luo, J.; van Loo, B.; Kamerlin, S. C. *FEBS Lett.* **2012**, *586*, 1622.
(95) Andrews, L. D.; Zalatan, J. G.; Herschlag, D. *Biochemistry* **2014**, *53*, 6811.
(96) Bobyr, E.; Lassila, J. K.; Wiersma-Koch, H. I.; Fenn, T. D.; Lee, J. J.; Nikolic-Hughes, I.; Hodgson, K. O.; Rees, D. C.; Hedman, B.; Herschlag, D. *J. Mol. Biol.* **2012**, *415*, 102.
(97) O'Brien, P. J.; Herschlag, D. *J. Am. Chem. Soc.* **1999**, *121*, 11022.
(98) Zalatan, J. G.; Catrina, I.; Mitchell, R.; Grzyska, P. K.; O'brien, P. J.; Herschlag, D.; Hengge, A. C. *J. Am. Chem. Soc.* **2007**, *129*, 9789.

DOI: 10.1021/jacs.6b06186
J. Am. Chem. Soc. 2016, 138, 14273−14287